IEEE/CSC & ESAS SUPERCONDUCTIVITY NEWS FORUM (global edition), January 2016.
MT-24 preprint 4OrAA_01. Submitted to *IEEE Trans. Appl. Supercond.* for possible publication.

1

In-depth Induction Heating of Large Steel Slabs by means of DC Saturating Field produced by SC Coils

Antonio Morandi, *Senior Member, IEEE*, and Massimo Fabbri

Abstract—The feasibility of an innovative in-depth AC induction heating method for large steel slabs is investigated. Beside the AC field, which induces the heating currents, a large DC magnetic field is also applied which brings the material to saturation. Due to the saturation the permeability is reduced by orders of magnitude and the penetration depth is drastically increased, thus making it possible a much faster and uniform heating. In order to produce the field needed for the saturation of common steels work piece, lossless DC superconducting magnets need to be employed.

The possible layout of the AC induction heater which employs magnetic saturation (Saturated AC Induction Heater) is discussed. The concept design of the superconducting magnet needed is carried out based on present state of the art superconducting materials. The performance of the saturated AC induction heater is investigated numerically and compared with the case of no magnetic saturation.

Index Terms—Induction heating, Temperature control, Steel slab, Saturation magnetization, Superconducting magnets, MgB₂.

I. INTRODUCTION

INDUCTION HEATING is widely used in industry for heating metals before hot workings (hot rolling, forming, extrusion, forging, etc.) [1]. The advantages of the induction heating over the heating by gas furnaces include absence of on-site CO_2 emission, fast operation, high surface quality, possibility to work in any processing atmosphere (including vacuum), contact-less operation and controllability [1]-[4].

Metal work-pieces (slabs, blooms, bars, and billets) are heated by induction until they reach a high enough temperature which creates proper conditions for plastic deformation [2]. Due to the skin effect, 87 % of thermal power injected during the process is produced in a layer located at the surface of the work-piece. The thickness of this layer is the penetration depth δ, which depends on the frequency *f* of the applied AC field and the electric resistivity ρ and the magnetic permeability μ of the processed material [3]:

$$\delta = \sqrt{\rho / \pi f \mu} \qquad (1)$$

High temperature uniformity at the end of the process is a mandatory requisite in industrial heating for hot workings. Short heating time is also strictly required in order to achieve high productivity. Appropriate uniformity and productivity can be easily reached in induction heating of non-magnetic metals such as aluminum, copper, silver or brass thanks to the large penetration depth, which allows the heat to penetrate deep within the material, combined with the high thermal conductivity. Thanks to the in-depth heating, satisfactory uniformity and productivity can also be obtained for non-magnetic metals with poor thermal conductivity (stainless steel, titanium and tungsten), provided that appropriate geometry and operating frequency are chosen for the AC coil [4]. However, when common steels, which are ferromagnetic from room temperature up to the Curie temperature (770°C), are considered, a very low penetration depth is obtained and heat generation is mostly confined at the surface. The heating of the work-piece's core is obtained via thermal diffusion only. This leads to slow process and large temperature gradients from surface to core. The process is further slowed down by the need to arrest it periodically and/or to reduce the power to allow homogenization and to avoid that excessive temperature is reached at the surface. This prevents cracking or even local melting, especially for high alloyed steels [5] and is particularly important for work-pieces with rectangular cross sections where electromagnetic end- and edge-effects can produce intense power concentration [1], [2], [6] - [9]. Due to these reasons, when real-world magnetic steel slabs or blooms with typical thickness in the range 0.2 - 0.3 m, width in the range 0.9 - 1.5 m and length in the range 4 – 11 m are considered [10], the heating by gas furnaces is the common solution [5], [11]-[16].

The feasibility of an innovative induction heating method for large steel slabs is investigated in this paper. The idea is to apply, beside the AC field which induces the heating currents, a large DC magnetic field which brings the material to saturation. Due to the saturation the permeability is reduced by orders of magnitude and the penetration depth is increased by a factor from 50 to 100 (depending on the temperature and the frequency), thus making it possible a much faster and uniform heating. It is be considered, however, that in order to produce saturation of common steels, a magnetic field of at least 2 T must be applied all over the volume of the processed slab. Such a relatively high field over such a large volume cannot be produced by means of permanent magnets. Furthermore, its generation by means of conventional electromagnets would require unpractical amount of copper and supply power. Fortunately, the saturating field can effectively be produced by means of superconducting magnets. Thanks to the DC operation no significant AC loss is generated in the magnet, which can hence be maintained in operation with affordable cooling power. Therefore, superconductivity is the enabling

IEEE/CSC & ESAS SUPERCONDUCTIVITY NEWS FORUM (global edition), January 2016.
MT-24 preprint 4OrAA_01. Submitted to *IEEE Trans. Appl. Supercond.* for possible publication.

2

technology for induction heating of large steel slabs.

This paper is organized as follow: the usual requirements of the heating process of common magnetic steels are reviewed in section II. The physical properties of the steel are examined in section III and the effect of applying magnetic saturation on the penetration depth is quantitatively assessed. A possible layout of the AC induction heater which employs magnetic saturation (hereafter Saturated AC Induction Heater) is discussed in section IV. The concept design of the superconducting magnet needed for the implementation of the heater is carried out in section V based on present state of the art superconducting materials. Finally, the performance of the saturated AC induction heater is investigated numerically and compared with the case of no magnetic saturation. The main assumptions of the numerical model are discussed in section VI. Results are presented in section VII.

II. REQUIREMENTS OF THE HEATING PROCESS

The induction heating of a magnetic steel slab for hot milling is considered in this paper. The average temperatures on the volume and surface of the slab, denoted with T_V and T_S respectively, are considered for evaluating the performance of the heating process. The temperature T_{core} at the center of the slab is also considered. A further important indicator is the surface-to-core temperature difference in the slab, denoted with ΔT. Finally, the maximum and the minimum temperature at any point of slab during the heating process, denoted with T_{max} and T_{mim} respectively, are also considered. We report that conventional induction heating of magnetic steels is commonly subdivided in two (or more) stages with different amplitude of the applied field, frequency and duration [2]. Increased magnitude and frequency are used as soon as the Curie temperature is reached at all point, in order to inject a greater power in the slab and obtain a faster heating. The same field and frequency cannot be used below the Curie temperature since excessive temperature gradients can occur near the surface which can produce cracking.

The requirements of the heating process are listed in Table I. The final temperature of the slab is between 1150°C and 1250°C[1] [12], [13]. This requirement must be fulfilled by the average temperatures T_V and T_S, and by the core temperature T_{core}. Moreover, in order to avoid local melting, an upper bound of 1350°C is set on the maximum temperature T_{max} [13], [16]. The required surface-to-core temperature ΔT, must be lower than 25°C at the end of the heating and must not overcome 380°C during the process [2], [7], [16][2]. Further non-mandatory objectives, which are also listed in Table I, are also assigned in order to comply with good heating practice. The bounds on T_{max} and T_{mim} at the end of the heating are set in order to minimize the soaking time needed for thermal

equalization, that is to satisfy the primary requirement on ΔT [2], [7]. A limit of 1 hour is usually set on the total heating time in order to obtain acceptable productivity of the steel plant. Lower or greater bounds are possible depending on the type of steel, the geometry of the work-piece and the initial temperature [7], [8], [12], [14], [17].

TABLE I
REQUIREMENTS OF THE HEATING PROCESS FOR MAGNETIC STEEL SLAB

	Primary objectives
Average volume temperature at the end of the process	1150 °C < T_V < 1250 °C
Average surface temperature at the end of the process	1150 °C < T_S < 1250 °C
Temperature at the core at the end of the process	1150 °C < T_{core} < 1250 °C
Maximum temperature during the process	T_{max} < 1350 °C
Surface to core Temperature difference at the end of the process	ΔT < 25 °C
Surface to core Temperature difference during the process	ΔT < 380 °C
	Secondary objectives
Maximum temperature at the end of the process	T_{max} < 1300 °C
Minimum temperature at the end of the process	T_{min} > 1100 °C
Heating time	< 60 min

III. PHYSICAL PROPERTIES OF THE STEEL

Common cast steel is considered for the present analysis. A mass density of 7870 kg/m^3 is assumed. All physical properties of the processed steel strongly depend on the temperature. Electrical resistivity, specific heat and thermal conductivity of the considered steel have been taken from [18]. The electrical resistivity increases non-linearly from 0.14 μΩ·m at room temperature up to 1.26 μΩ·m at the melting temperature, i.e. 1350°C. The specific heat increases from 455 J/kgK at room temperature up to 764 J/kgK at the melting temperature, exhibiting a pronounced maximum of 1130 J/kgK near the Curie temperature, i.e. 770°C. The thermal conductivity decreases from 71 W/m·K at room temperature up to 33 W/m·K at the melting temperature, with a minimum of 27 W/m·K near the Curie point.

Fig. 1 shows the B-H curves for various temperatures in the range from room temperature up to the Curie point [19]. It can be seen that the decrease of the magnetic behavior with the temperature is smooth at the beginning and is quite sharp in the proximity of the Curie temperature, where the material becomes non-magnetic. Fig. 2 shows the AC penetration depth at 50 Hz when a DC field of amplitude in the range 0 - 2.5 T is superimposed. Values reported are obtained from (1) wherein the magnetic permeability μ at any given temperature is obtained from by linearizing the B-H curves of Fig. 1 around the value of the applied DC field. It can be seen from Fig. 2 that if no DC field is applied then deep penetration is obtained only above the Curie temperature. We see also that if significant penetration is to be obtained at low temperature then a DC field of at least 2 T needs to be applied.

---

[1] This is the most common range. However, a larger temperature range can be applied depending on the chemical composition of the steel [2], [6].

[2] It is worth to point out that the limit on ΔT at the end of the process depends on the post-heating operations and can be larger of 25 °C in some cases [2], [8], [9], [12], [14]. Furthermore, the limit on ΔT during the process is due to the need to avoid cracking and depends on the mechanical properties of the steel. Usual values are in the range 150–380 °C [5], [15].

IEEE/CSC & ESAS SUPERCONDUCTIVITY NEWS FORUM (global edition), January 2016.
MT-24 preprint 4OrAA_01. Submitted to *IEEE Trans. Appl. Supercond.* for possible publication.
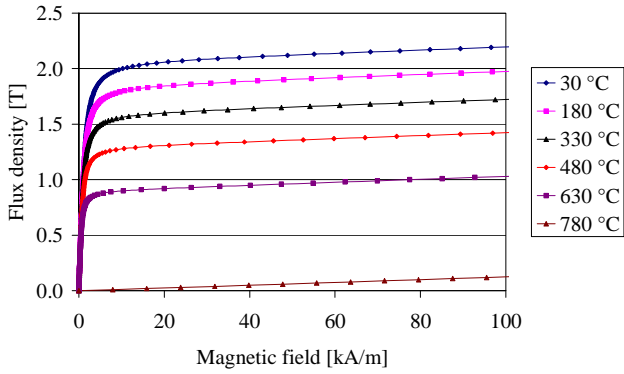
3

Fig. 1. Calculated B-H curves of the considered steel from room up to the Curie temperature.
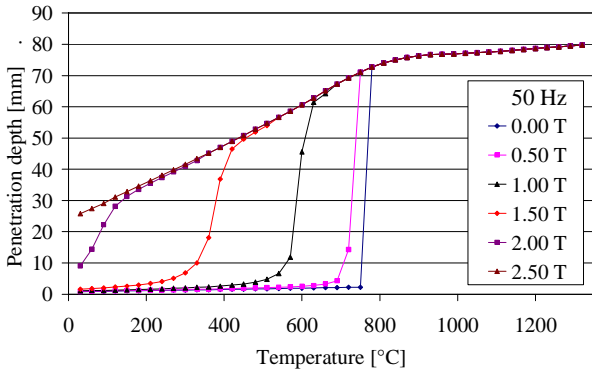

Fig. 2. Penetration depth at 50 Hz in the considered steel from room temperature up to melting temperature for different values of the DC saturating field.

IV. LAYOUT OF THE HEATER

The induction heating of a steel slab with 200 mm thickness, 1000 mm width and 5 m length is considered. The slab is made of common magnetic steel. Fig. 3 shows the 3D view of the heater. A section view of the heater with more information about the main dimension of the components is shown in Fig. 4. The slab is placed in the center of the heater. A refractory hull, which is not shown in Fig. 3, is used to enclose the slab all over its length in order to minimize heat loss and to protect the surrounding apparatus form excessive heat radiation. A refractory-coated skid system is used for the injection and the extraction of the slab. A water-cooled copper coil is placed at the outer of the refractory hull in order to produce the AC field. For simplicity one single AC coil (5.5 m long) which extend all over the slab length is considered even if industrial AC coils are usually split into multiple units [6]. A thickness of 20 mm is chosen for the AC coil. A maximum current density of 8 A/mm^2 is needed for producing the maximum AC field magnitude of 200 mT which is required for the heating process (see section VII). The current of the AC coil flows parallel to the *y-z* planes and the field produced is parallel to the long dimension of the slab (*x*-direction). A DC field is applied in *z* direction in order to saturate the slab. This saturating field is produced by a split superconducting coil made of two identical racetracks coils placed above and below the AC coil, as its shown in Fig. 3. Split configurations

allows an easy injection and extraction of the Slab. Non-spilt layouts, which substantially simplify the SC coil are possible, in principle, but they require much more complex injection and extraction system and are not considered. A total gap of 85 mm exists between the DC coil and the AC one, which is needed for allocating the cryostat. The DC coil can produce a magnetic field of about 2 T in air at the center of the heater. The field produced is greater than 2 T all over the volume occupied by the slab. The details of the DC superconducting coil are discussed in section V. We stress that if saturation of the steel is produced in one direction then the effective permeability ($\partial B_i/\partial H_i$, $i = x, y, z$) is reduced to μ_0 in all the directions. This means that the penetration depth of the currents induced in *y-z* plane by the AC coil is greatly increased due to the saturating field which is applied perpendicular to this plane by the split DC coil. We point out that orthogonality between AC and DC field is essential for decoupling the two coils. In fact, if the coils are coupled than AC loss are induced in the DC coil by the AC field. Furthermore, high AC voltage is iduced at the terminals of the coil connected with the DC power supply due to the transformer effect.
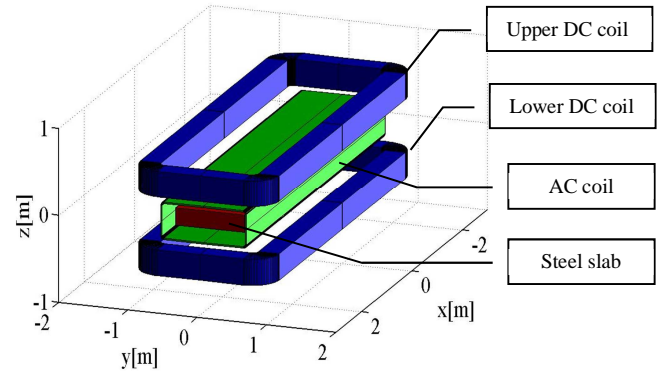

Fig. 3. 3D view of the heater. A steel slab with 200 mm thickness, 1000 mm width and 5 m length is considered. AC and DC coils are shown. Refractory and the cryostat are not shown.
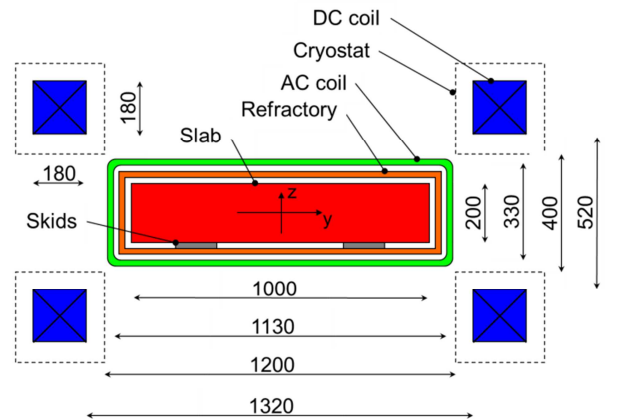

Fig. 4. Section view of the heater. Refractory and the cryostat are shown. Main geometrical data are also reported.

IEEE/CSC & ESAS SUPERCONDUCTIVITY NEWS FORUM (global edition), January 2016.
MT-24 preprint 4OrAA_01. Submitted to *IEEE Trans. Appl. Supercond.* for possible publication.

4

V. DESIGN OF THE SUPERCONDUCTING DC COIL

A commercial MgB_2 wire is considered for the design of the split superconducting coil. This superconductor is available at the industrial level at competitive costs. A Rutherford assembly is considered for the MgB_2 wires. Feasibility of multi-strand Rutherford cables made of MgB_2 round wires has been demonstrated [20]. The possibility to replace the MgB_2 with more performing 2G-HTS materials (YBCO Coated Conductors) can be considered, in order to optimize the coil, as soon as these material becomes available at more reduced costs. The procedure described in [21] is used to carry out the design of the coil. More details about the considered MgB_2 conductor are also reported therein. The main characteristics of the coil are reported in Table II. It can be appreciated from the table that a very complex magnet is obtained. In particular, about 900 km of MgB_2 wire are needed which, based on today's quotation, are worth from 1 to 2 M€. It is to be noted, however, that if heavily water-cooled copper coil (with $J_{Cu} = 10$ A/mm^2) is considered instead of the superconductor, then about 80 tons of copper are need which are worth about 450 k€. Moreover, the Joule losses of this coil would be about 17 MW. When compared with the typical heating power injected in the slab, which is in the order of 3-6 MW (see section VII), these losses would make the process unpractical in terms of efficiency.

We stress that much simpler DC coil can be obtained if a flat (rectangular shaped) solenoid layout rather than a split geometry is considered. However, as this DC solenoid is to be perpendicular to the AC one in order to avoid AC loss and induced voltage, it requires a very complex system for inject and extract the slab. Feasibility of flat solenoid type needs to be evaluated in cooperation with final users.

TABLE II
MAIN CHARACTERISTICS OF THE SPLIT SUPERCONDUCTING DC COIL

Type of SC conductor	Round MgB_2 Wire 1.13 mm diameter
Operating temperature of the coil	16 K
Cross section of the coil	Square, side 180 mm
Number of wires of the Rutherford cable	10
Field at the center of the slab	2.0 T
Max field on the conductor	3.7 T
Current of the Coil	900 A
I/I_c ratio of the MgB_2 wire ratio at the max. field	0.65
Length of the coil	5.8 m
Width of the coil	2 m
Minimum curvature radius	85 mm
Inductance of the coil in air	143 H
Total stored energy of the coil in air	58 MJ
Total length of MgB_2 wire	895 km

VI. NUMERICAL MODEL

In order to analyze the induction heating of the slab the distribution of magnetic field, current density and temperature need to be calculated at any instant. These three problems are strongly coupled one to the other. In particular, the magnetic

field affects the local permeability, and hence it has a strong effect on the local distribution of currents induced by the AC coil. For calculating the solution we subdivide the slab in a finite number of 3D hexahedral elements and we solve the problems by using the same mesh as follows:

i. A time interval form t to $t+\Delta t$ is considered. At time t, given the distribution of temperature inside the slab, the distribution of magnetization produced by the applied DC field only is calculated by using the numerical approach developed in [22] - [24].

ii. The distribution of current density produced by the AC coil is calculated by means of the circuit approach developed in [22], [25]-[27]. To accomplish this step we linearize the B-H curves of the material (see Fig. 1) at the calculated DC field value, at any point of the slab. In essence we assume that the field produced by the AC coil and the induced current has a negligible influence on distribution of magnetic field inside the material. This is a reasonable assumption since the field of the AC coil is much lower than the applied DC field, and moreover it is further shielded by the induced currents. Since a linear problem is obtained we perform a complex steady AC analysis to find the solution.

iii. The power density inside the slab is obtained from the previous step and is assumed fixed during integration interval. The temperature distribution at the end of the integration interval (time $t + \Delta t$) is obtained by means of the circuit approach developed in [25] -[27]. The calculation is restarted from step i.

The numerical models used throughout steps i – iii have been validated against experimental results and benchmarks [22], [27]. A weak coupling is assumed, so that the magneto-static (with fixed temperature distribution – step i), electromagnetic (with fixed temperature and DC field distributions – step ii), and thermal (with fixed AC joule power density distribution – step iii) problems can be solved sequentially and independently. The boundary conditions of the thermal problem are obtained by assuming convective and radiating heat exchange of the slab with the air and the refractory envelope. A temperature independent emissivity equal to 0.6 was considered as suggested in [17]. The heat exchange coefficients due to natural convection were deduced using Churchill and Chu correlation for the vertical walls of the slab and McAdams correlation for the horizontal ones [28]. The temperature-dependent air properties were taken from [29]. The air temperature was assumed to be equal to the average temperature of the refractory on the inner walls of furnace. The temperature of the refractory walls was evaluated by solving the energy balance at each time step. In order to simplify the analysis the effects on the boundary conditions of the water-cooled skids were neglected [2], [5]. The temperature-dependent properties of the refractory were taken from [30].

We stress that for obtaining the solution of the electromagnetic problem (step ii) the differential permeability,

IEEE/CSC & ESAS SUPERCONDUCTIVITY NEWS FORUM (global edition), January 2016.
MT-24 preprint 4OrAA_01. Submitted to *IEEE Trans. Appl. Supercond.* for possible publication.

5

i.e. the derivative of the B-H curve, is needed in each element of the mesh. Since the B-H curve is obtained from a discrete set of points care must be used in the interpolating functions in order to avoid unphysical value of the derivative which could lead to non-physical solutions. In order to avoid this problem the discrete B-H data were interpolated by using Bezier curves. A controllable initial value of the permeability was thus obtained and oscillations were avoided [31]. The obtained values of the relative differential permeability were smooth and decreased with the temperature and the field starting from the maximum value of 1000. We also point out that the maximum size of the elements of the mesh needs to be at most comparable with the lowest penetration depth that occurs in the slab during the heating (0.5 mm). Due to the large dimension of the slab a very large number of elements is hence obtained. In order to keep the numerical problem within acceptable limits we have used a fine discretization only along the thickness of the slab (z axis), whereas in the other two dimension we have used a coarse discretization. Advanced numerical approach based on adaptive mesh near the mobile front which separates the magnetic and the non-magnetic zone should be applied for more refined calculations.

VII. RESULTS AND DISCUSSION

A. Slab heating without DC saturation field

Fig. 5 shows the temperatures in the slab during the heating without DC saturating field. The calculated heating times agree well with the values reported in literature both for the second stage only and for the whole heating process [5], [7]. As it is common for conventional induction heating of magnetic steel the process is subdivided in two stages with different amplitude and frequency of the applied field [2]. An AC field with 90 mT / 50 Hz is applied during the first stage which ends after 47 min, when the Curie temperature is reached at any point of the slab. An AC field with 180 mT / 110 Hz is applied during the second stage, which begins at 47 min and ends at 76 min when the primary objectives defined in Table I are met. The power grid frequency is used in the first stage while, during the second stage, a higher frequency (110 Hz) is used to increase the heating power, provided that the corresponding penetration depth is comparable with the slab thickness [5], [8]. The amplitude and the frequency of the AC field during the two stages were chosen by trial and error until the primary requirements of the heating were fulfilled with the minimum heating time. The thermal power input changes with time during the process, as it shown in Fig. 6. A much higher steady power can be observed during the second stage (though a power peak is obtained at the beginning of the heating during the first stage).

The secondary objectives, both on the minimum and maximum temperatures and on the heating time, are not met. The requirement on minimum and maximum temperatures could be achieved with a soaking phase. However, the long heating time can hardly be reduced, since it is due to the primary constraint on the surface-to-core temperature difference which is quite high, as shown in Fig. 6. In order to reduce the temperature difference it would be necessary to reduce the frequency below 50 Hz or to reduce the AC field

magnitude. In both cases the heating power would decrease and the total heating time would increase.
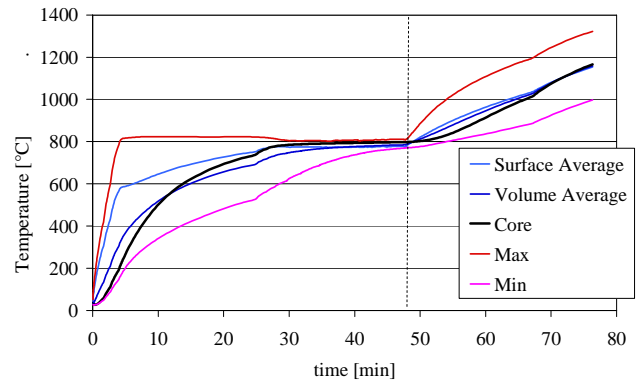

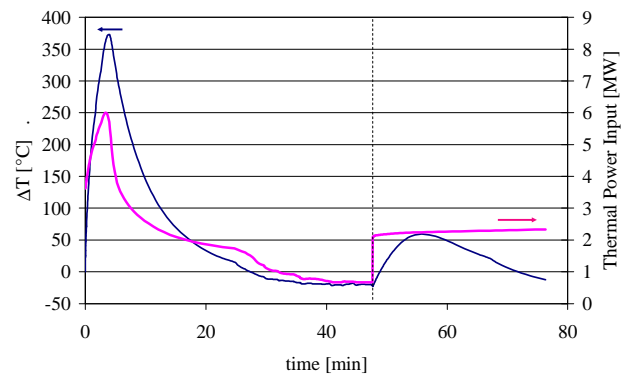Fig. 5. Temperatures during the heating of the slab without DC saturation field.

Fig. 6. Surface-to-core temperature difference and thermal power input in the slab during the heating without DC saturation field.

B. Slab heating with 2 T DC saturation field – solution 1

Fig. 7 shows the temperatures in the slab during the heating with 2 T DC saturation field aplied. An AC field with 200 mT / 300 Hz is applied during the first stage which ends after 21 min, when the maximum allowable temperature of 1350 °C is reached in the slab. An AC field with 200 mT / 50 Hz is applied during the second stage, which begins at 21 min and ends at 36 min when the primary objectives defined in Table I are met. Also in this case the amplitude and the frequency of the AC field and during the two stages were chosen by trial and error until the primary requirements of the heating were fulfilled with the minimum heating time. A remarkable reduction of the heating time of about 50 % is obtained with respect to the case without DC field. We note that, thanks to the slab's saturated produced by the DC superconducting coil, the AC excitation at 300 Hz can be used during the first stage without the risk of hot spot at the surface of the slab. As it is shown in Fig. 8, a larger thermal power is obtained due to the higher frequency which allows to greatly speed up the heating up to the maximum temperature [2]. We report that the present heating process allow also the fulfillment of the secondary objectives if the second stage is continued up to 43 min.

IEEE/CSC & ESAS SUPERCONDUCTIVITY NEWS FORUM (global edition), January 2016.
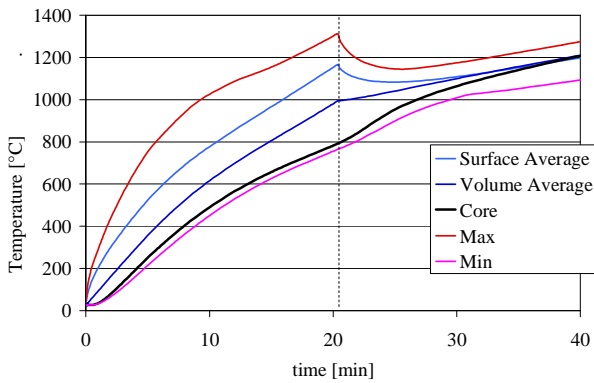MT-24 preprint 4OrAA_01. Submitted to *IEEE Trans. Appl. Supercond.* for possible publication.

6

Fig. 7. Temperature in the slab during the heating of the slab with 2 T DC saturation field.
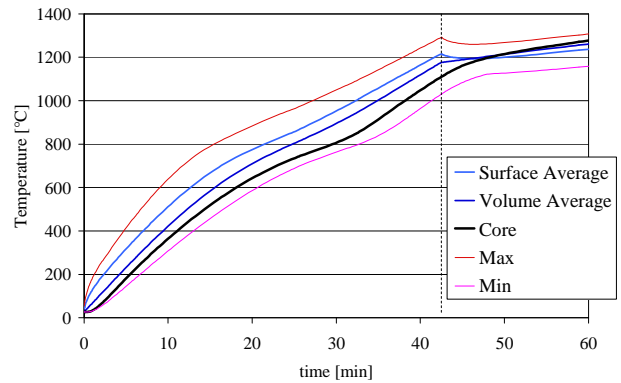

Fig. 9. Temperature in the slab during the heating of the slab with 2 T DC saturation field.
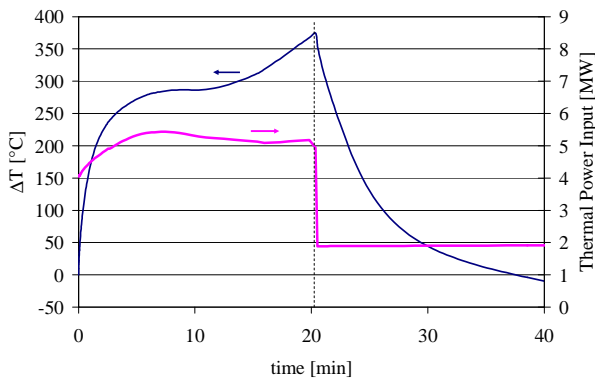

Fig. 8. Surface-to-core temperature difference and thermal power input in the slab during the heating with 2 T DC saturation field.
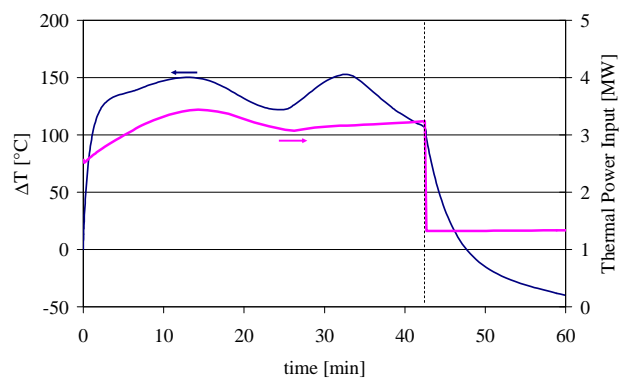

Fig. 10. Surface-to-core temperature difference and thermal power input in the slab during the heating with 2 T DC saturation field.

C. *Slab heating with 2 T DC saturation field – solution 2*

In the cases investigate so far, both with and without the DC saturating field, the limiting factor is the constraint on the surface-to-core temperature difference during the heating process. In fact, as it can be seen in Figs 6 and 8, the maximum allowable limit ($\Delta T < 380°C$, see table I) is reached in both the processes. With the aim to strongly reduce the surface-to-core temperature difference a further process is considered here. This process uses saturating DC field of 2 T and only uses the 110 Hz frequency. A reduced magnitude of the AC field is used during the second stage in order to reduce the power. Fig. 9 shows the temperatures in the slab during the heating. The first stage lasts 42 min with AC field of magnitude 200 mT at 110 Hz. The second stage begin at 42 min with AC field of magnitude 130 mT at 110 Hz. The process ends at 46 min when the primary and the secondary objectives defined in Table I are met. The heating time is higher than in the previous case but the surface-to-core temperature difference is 150 °C only, as shown in Fig. 10. This process may be suitable for the heating of special steels with very strict requirement on the surface-to-core temperature difference.

VIII. CONCLUSION

Saturation of magnetic steel during AC induction heating allows to increase the penetration depth and to obtain heating processes which satisfy all the requirements in terms of maximum allowable temperatures, gradients and heating times. When common steel work-piece are considered a magnetic field of at least 2 T needs to be applied on a bore of typically 0.5 m in order to produce saturation. Such a field cannot be produced by means of the copper coils due to the large amount of material and the unaffordable power required. Conversely, though non trivial, this field can effectively be produced by means of superconducting magnets based on present state of the art SC materials. Superconductivity is the enabling technology for fast and efficient induction heating of magnetic steels.

REFERENCES

[1] R.C. Goldstein and V.S. Nemkov, "Design principles for induction heating and hardening," in *Handbook of Metallurgical Process Design*, L. Xie , K. Funatani , and G. E. Totten, Eds. Boca Raton, Florida: CRC Press, 2004, pp. 591-640.

[2] Y. Pleshivtseva and E. Rapoport, *Optimal Control of Induction Heating Processes*. Boca Raton, Florida: CRC Press, 2006, pp. 1-34.

[3] V.I. Rudnev, R.L. Cook, D.L. Loveless, and M.R. Black, "Induction heat treatment: basic principles, computation, coil construction, and design considerations," in *Steel Heat Treatment Handbook*, 2rd ed., G. E. Totten, Ed. Boca Raton, Florida: CRC Press, 2006, pp. 306-310.

[4] V. Rudnev, D. Loveless, K. Schweigert, P. Dickson, and M. Rugg, "Efficiency and temperature considerations in induction re-heating of

IEEE/CSC & ESAS SUPERCONDUCTIVITY NEWS FORUM (global edition), January 2016.
MT-24 preprint 4OrAA_01. Submitted to *IEEE Trans. Appl. Supercond.* for possible publication.

7

bar, rod and slab," *Industrial Heating* (USA), June 2000. [Online.] Available: http://www.industrialheating.com Accessed on 10 Sept. 2015.

[5] S. Chen, "Modeling for Reheat Furnace Practices," in *Flat-Rolled Steel Processes Advanced Technologies*, V. B. Ginzburg, Ed. Boca Raton, Florida: CRC Press, 2009, pp. 99-114.

[6] V. Rudnev, "Successful induction heating of RCS billets," *Forge*, pp. 15-18, July 2008. Available: http://www.forgemag.com

[7] N.V. Ross, "A system for induction heating of large steel slabs," *IEEE T Ind Gen A*, vol. IGA-6 (5), pp. 449-454, Sept./Oct. 1970.

[8] C.D. Kramer, "Induction Heating Steel with 60 Cycles," *IEEE T Ind Appl* vol. 73(6), pp. 353-357, Jan. 1955.

[9] D.G.Hatchard, "Induction heating of bars and semifinished steel," *IEEE T Ind Gen A*, vol. IGA-2 (5), pp. 246-352, Sept./Oct. 1966.

[10] [Online.] http://www2.outokumpu.com Accessed on 10 Sept. 2015.

[11] G. E. Totten, D. Pye , and N. Gopinath, "Heat treatment equipment," in *Steel Heat Treatment Handbook*, 2rd ed., G. E. Totten, Ed. Boca Raton, Florida: CRC Press, 2006, pp. 14-43.

[12] A. Steinboeck, D. Wild, and A. Kugi, "Nonlinear model predictive control of a continuous slab reheating furnace," *Control Eng Pract*, vol. 21, pp. 495-508, 2013.

[13] L. Balbis, J. Balderud, and M. J. Grimble, "Nonlinear Predictive Control of Steel Slab Reheating Furnace," Proc. 2008 American Control Conference, Seattle, Washington, June 11-13, 2008, pp.1679-1684.

[14] W.H. Chen, M.R. Lin, and T.S. Leu, "Optimal heating and energy management for slabs in a reheating furnace," *J Mar Sci Technol*, vol. 18(1), pp. 24-31, 2010.

[15] N.K. Nath, P.S. Assis, and A. Chowdhury, "Numerical simulation of ingot and concast steel reheating in batch and continuous type furnace to optimize energy efficiency, quality and productivity," Proc. of the Int. Conf. on Science and Technology of Ironmaking and Steelmaking (STIS 2013) Jamshedpur, India, December 16-18, 2013. [Online.] Available: http://eprints.nmlindia.org/7019 Accessed on 10 Sept. 2015.

[16] N. Wang, Z. Wen, and F. Su, "Optimal heating and energy management for the reheating furnace using oxygen enhanced combustion," Proc. of the 2013 AIChE Annual Meeting, San Francisco, CA, November 3-8, 2013. [Online.] Available: http://www3.aiche.org Accessed on 10 Sept. 2015.

[17] R. Mei, C. Li, X. Liu, B. Li, and B. Han, "Modeling of slab induction heating in hot rolling by FEM," *Engineering*, vol. 3, 2011, pp. 364-370.

[18] A. Tsalaf, *Combined properties of conductors*, Amsterdam: Elsevier Scientific Publishing Co., 1981, pp.536-589.

[19] M. Morishita, N. Takahashi, D. Miyagi, and M. Nakano, "Examination of magnetic properties of several magnetic materials at high temperature," *Przeglad Elektrotechniczny* (Electrical Review), vol. 87 (9b), 2011, pp. 106-110. [Online.] Available: http://www.red.pe.org.pl Accessed on 10 Sept. 2015.

[20] L. Kopera, P. Kovac, I. Husek, and T. Melisek, "Rutherford cable made of single-core MgB2 wires," *Supercond Sci Technol*, vol. 26, 2013. Paper ID: 125007.

[21] A. Morandi, B. Gholizad and M. Fabbri, "Design and performance of a 1 MW – 5 s, High Temperature Superconductor Magnetic Energy Storage system," 2015, *Supercond Sci Technol*, in press.

[22] A. Morandi, M. Fabbri, P. L. Ribani, "A modified formulation of the volume integral equations method for 3D magnetostatics", *IEEE T Magn*, vol. 46 (11), pp.3848-3859, 2010.

[23] A. Pellecchia, D. Klaus, G. Masullo, R. Marabotto, A. Morandi, M. Fabbri, C. Goodhand, and J.Helm, "Magnesium diboride magnets for core bias flux generation in pre-saturated core type fault current limiters," *IEEE T Appl Supercond*, submitted for publication. [Int Conf. on Magnet Technology 24, October18-23, 2015, Seoul, Korea. Paper ID. 0603NP0063]

[24] M. Fabbri, "Magnetic flux density and vector potential of uniform polyhedral sources", *IEEE T Magn*, vol. 44 (1), pp. 32-36, 2008.

[25] M. Fabbri, A. Morandi, F. Negrini, P. L. Ribani, "Temperature dependent equivalent circuit of a magnetic-shield type SFCL", *IEEE T Appl Supercond*, vol. 15 (2), pp. 2078-2081, 2005.

[26] A. Morandi, M. Fabbri, P. L. Ribani, "Coupled electromagnetic-thermal model and equivalent circuit of a magnetic shield type SFCL", *IEEE T Appl Supercond*, vol. 23 (3), 2013. Paper ID. 5602705.

[27] M. Fabbri, M. Forzan, S. Lupi, A. Morandi, P. L. Ribani, "Experimental and numerical analysis of dc induction heating of aluminum billets", *IEEE T Magn*, vol. 45 (1), pp.192-200, 2009.

[28] J. R. Welty, C. E. Wicks, R. E. Wilson, and G. L. Rorrer, *Fundamentals of Momentum, Heat and Mass Transfer*, New York: Wiley, 2007, pp.300-301.

[29] [Online.] http://www.engineeringtoolbox Accessed on 10 Sept. 2015.

[30] T. Shimizu, K. Matsuura, H. Furue, and K. Matsuzak, "Thermal conductivity of high porosity alumina refractory bricks made by a slurry gelation and foaming method," *J Eur Ceram Soc*, vol. 33, pp. 3429-3435, 2013.

[31] M.E. Mortenson, *Mathematics for Computer Graphics Applications*, 2rd ed. New York: Industrial Press Inc., 1999, pp.264-275.